



Green synthesis of Silver-iron-zinc oxides nanocomposite via *Embelia schimperia* leaf extract for photo-degradation of antibiotic drug from pharmaceutical wastewater

Defar Getahun Gizachew¹ · Edo Begna Jiru¹ · Tsigab Tekle'Ab¹ · Yigezu Mekonnen Bayisa¹ · Tafere Aga Bullo¹

Received: 31 October 2023 / Accepted: 6 August 2024 / Published online: 31 August 2024
© The Author(s) 2024

Abstract

The co-precipitation approach is used in the current study to create an environmentally friendly Ag/Fe/ZnO nanocomposites utilizing an aqueous leaf extract of *Embelia schimperia*. The synthesized nanocomposite was characterized using Fourier-transform infrared, UV, X-ray, UV-vis, DLS, TGA, and SEM to determine its functional group, structure, bandgap energy, size distribution, a mass of loss, and energy gain or loss, and morphological structure, respectively. The bioactive components of *Embelia schimperia*, synthesized Ag/Fe/ZnO NCs and degradation of Amoxicillin via photocatalyst were assessed. The response surface methodology of central composite design (CCD) was used to examine and optimize the effects of three independent variables on the degradation of Amoxicillin under visible light. According to the experimental findings, the maximum photocatalytic degradation efficiency was achieved at green synthesized Ag/Fe/ZnO NCs dosage of 100 mg, a concentration of Amoxicillin of 30 mg/L and a radiation time of 180 min. Their findings show that *Embelia schimperia* extract-derived Ag/Fe/ZnO nanocomposites is a promising alternative for degradation of pharmaceuticals contamination of wastewater via photocatalytic under the given conditions.

Keywords Ag/Fe/ZnO nanocomposites · Central Composite Design · Degradation of Amoxicillin · *Embelia schimperia* leaves · Photocatalyst

Introduction

Water is very useful for all humans, animals, plants, and the whole ecosystem. However, to use the water keeping, the quality of this water is very important. Nowadays, water is contaminated by different contaminates: Natural, physical, chemical, and biological contaminants such as salt, sand dust, organic, inorganic, bacteria, protozoa, viruses, and parasite contaminants (Pandit & Kumar 2019; Sharma et al. 2018). Chemical contaminants are among the most abundant pollutant in water sources (Bozorg-Haddad et al. 2021; Khan et al. 2020). Pharmaceutical waste is one of the major worrying emerging contaminants, which arise from pharmaceutical industries that are biologically active compounds that daily life used (Bayisa et al. 2021; Costa et al. 2019;

Kharissova et al. 2019). When the effluent from Pharmaceuticals waste is discharged into the water stream, that bring significant risks posed, leading to genotoxic, mutagenic, and eco-toxicological effects on plants, animals, humans, microbial, living things, and others (Samal et al. 2022). This pharmaceutical wastewater contained different organic and inorganic pollutants, which contaminate water (Aththanayaka et al. 2022). To treat this pharmaceutical wastewater, different methods and strategies are there from different sources of raw material (Khan et al. 2020). According to different scholars stated treatments of pharmaceutical wastewater by green synthesized metal oxide nanocomposites (MONCs), which is better than another, are in terms of cost, time, efficiency, and safety (Afolalu et al. 2022; Bullo & Bayisa 2022; Khan et al. 2020; Kharissova et al. 2019). Among other magnetic metals, Ag, Fe, and Zn get great attention due to their unique optoelectronic properties, shapes, sizes, and large specific surface areas (Immanuel et al. 2019). Moreover, Ag is easily produced because of its chemical inertness, durability to surface oxidation, better shape control, size, and relative stability when compared to other alloys (Ishak et al.

✉ Yigezu Mekonnen Bayisa
yigezu.mekonnen@ju.edu.et

¹ School of Chemical Engineering, Jimma Institute of Technology, Jimma University, Jimma, Oromia, Ethiopia

2019; Samal et al. 2022) and induce oxidative stress and cellular toxicity by producing reactive oxygen species (ROS). In addition, more ROS can be produced by the ZnO and Ag nanocomposite, which can also have a cumulative influence on photocatalysis, antibacterial, and anticancer properties. Likewise, because of its superparamagnetic and distinctive physicochemical characteristics, iron nanoparticles are a versatile remediation material. They also have good electron-donating qualities and are quite reactive in water at ambient conditions.

The green synthesis methods include the synthesis of nanomaterials from the plant, bacterial, fungal species, algae, and yeast (Salem & Fouda 2021). Green synthesis methods of nanocomposite from the plant are most appropriate than bacterial, yeast, and fungi (Singh et al. 2018). Plant is a better source of nanocomposite as a reducing agent than bacteria, yeast, fungi, and algae in terms of efficiency, reusability, ecofriendly and cost (Aththanayaka et al. 2022; Jeevanandam et al. 2022). Thus, in this study, Ag–Fe–ZnO nanocomposite was synthesized using *Embelia schimperia* leaf as a reducing agent and AgNO_3 , Fe_2NO_3 , ZnNO_3 as the precursor. The synthesized nanocomposite was used for the treatment of pharmaceutical wastewater.

Material and methods

Materials and reagents

The silver nitrate (AgNO_3 , 99%), zinc acetate hexahydrate ($\text{Zn}(\text{CH}_3\text{COO})_2 \cdot 2\text{H}_2\text{O}$, 98%, extra pure), and iron chloride (FeCl_3 , 99%), produced by Loba Chemicals Pvt. Ltd in India, was purchased from Atomic Educational Materials Supply PLC in Addis Ababa, Ethiopia. *Embelia schimperia* leaf was acquired from Jimma Institute of Technology Campus, Southwestern Oromia, Ethiopia. All the other chemicals were analytical reagent grade and bought from Al-Chem-Supply Kirkos Ltd. in Addis Ababa, Ethiopia. All reagents used in this study were pure analytical grade.

Preparation of plant extract

Embelia schimperia leaves were collected from the Jimma Institute of Technology campus and washed with distilled water to remove sludge and dust. The collected raw materials (leaves) were air-dried for a week and grinded with a mortar and pestle to small sizes. It was then kept in a clean, dry place and ready for extraction. After one week, 20 g of crushed dried leaves and 200 ml of deionized water were added to a 500-ml conical flask and mixed vigorously. The mixture was then heated at 70 °C for 45 min in a water bath, and then cooled to room temperature and filtered the extract with filter paper. The filtrate was used as a reducing and

stabilizing agent. The filtrate was stored at 4 °C for further use (Alwhibi et al. 2021; Biswal et al. 2020).

Qualitative phytochemical screening of *Embelia schimperia* leaf extract

The presence of alkaloids, glycosides, steroids, saponins, flavonoids, terpenoids, and tannins, among other things, was detected by a distinctive color shift in extracts using established techniques (Bayisa & Bultum 2022).

Test for Alkaloids To determine the alkaloid presence in leaf extract, 5 ml drops of Wagner's and Dragendorff's reagents were added to different 5 ml of the filtrate. Then, the color changed was observed (Bayisa & Bultum 2022).

Flavonoid Test The flavonoid presence in leaf extract was determined by taking 4 drops of concentrate HCl and magnesium ribbon, and added to 5 ml leaf extract (Bayisa & Bullo 2021).

Test for Terpenoids To determine the terpenoids presence in leaf extract, 2 ml of chloroform was added to 5 ml of leaf extract and waited for few minutes. Then, 3 ml of concentrate H_2SO_4 was added, and color changed was observed (Bayisa & Bullo 2021).

Test steroids 20 gm leaf extract was mixed with 200 ml of distilled water and heated for 45 min. After, the solution was cooled and filtered, 4 ml of chloroform added to 5 ml of leaf extract. Then, 3 ml of concentrate H_2SO_4 was added, and color changed was observed.

Test for Tannin: To determine the tannin presence in leaf extract, 5 ml of leaf extract was mixed with a few drops 5% of ferric chloride solution, and the color changed was observed (Siddiqui et al. 2021).

Test for Saponin: 5 ml of extract and 5 ml of distilled water were added and shaken vigorously in a graduated cylinder for 2 min lengthwise. Then, the shacked was waited for 5 min, and its layer foam height indicated the presence of saponins (Yadav & Agarwala 2011).

Test for Polyphenol A 3 drops of 3% of ferric chloride and 3 drops of 1% $\text{K}_3\text{Fe}(\text{CN})_6$ were added into 5-ml leaf extract. Then, the solution was shacked little, and color change was observed (Yadav & Agarwala 2011).

Test for Glycosides To 2 ml of extract, 3 ml of chloroform and 10% ammonia solution was added. Formation of pink color indicates presence of glycosides. Using Liebermann's test, crude extract was mixed with each of 2 ml of chloroform and 2 ml of acetic acid. The mixture was cooled in ice. Carefully concentrated H_2SO_4 was added (Bayisa & Bullo 2021).

Green synthesis of Ag/Fe/ZnO nanocomposites

Ag/Fe/ZnO nanocomposite was synthesized by using the hydrothermal process. Firstly, Ag/Fe/ZnO nanocomposite

was prepared from 0.1 M AgNO₃ solution, 0.1 M FeCl₃ solution and 0.1 M of Zinc acetate dehydrate were prepared separately. Prepared solutions were mixed together and the solution was stirred constantly. After the completed homogenization of the solution was precipitated was dried in a hot-air oven at 90 °C for 10 h, reduced to a powder, and calcined at 400 °C for 3 h in a muffle furnace to obtain pure Ag/Fe/ZnO nanocomposite (Bayisa et al. 2023; Biswal et al. 2020).

Nanocomposite characterization

The synthesized Ag–Fe–ZnO Nanocomposite was characterized by its size, shape, surface area, optical properties, and disparity using advanced instruments such as, DLSC, UV–Visible spectroscopy, XRD, FTIR, TGA, SEM, and BET.

Photocatalyst experiment

The photocatalytic effectiveness of Ag/Fe/ZnO NCs against Amoxicillin degradation was studied utilizing a 15 W LED lamp as a light source. Amoxicillin and catalyst were mixed to make a reaction suspension in a 250-ml beaker with a double-layer jacket. The temperature was kept constant at 25 °C throughout the studies. The photocatalytic degradation of Amoxicillin was measured using a 200-mL working solution having an Amoxicillin concentration, and Ag/Fe/ZnO NCs in 250-ml beaker. Then, solution was sonicated and magnetically agitated for 30 min in a dark room to ensure homogeneity. The solution was then irradiated with 15 W LED bulb visible light and constantly swirled with a magnetic stirrer. The sample was then collected every 30 min and centrifuged to separate the catalysts from the liquid before the absorbance measurement. The absorbance of each sample was determined after Amoxicillin was photocatalytically degraded. After the photocatalytic degradation of Amoxicillin, the absorbance of each sample after 30 min interval was measured using UV–visible spectroscopy. The percentage of photocatalytic degradation of those calculated by Eq. (1).

$$\%D = \frac{(C_0 - C_t)}{C_0} * 100\% \quad (1)$$

whereas % D = percentage of photocatalytic degradation.

C₀ = initial concentration of Amoxicillin.

C_t = concentration at time Amoxicillin.

Experimental design

For this study, Design Expert 13.8.0 software was used for Experimental data analysis (Bayisa & Teso 2021; Mekonnen 2021). The experimental design selected for this work is two-level three-factor response surface methodology

of the central composite design experiment model for the parameter variable Ag/Fe/ZnO NCs dosage, time and dosage of amoxicillin on the photocatalytic degradation of the efficiency.

Result and discussion

Phytochemical analysis

The phytochemicals found in the leaves are responsible for the formation of Ag/Fe/ZnO NCs. As a result, phytochemical assays on *Embelia schimperia* leaf extract were performed prior to NC synthesis. The extract was tested the presence of alkaloids, glycosides, steroids, saponins, flavonoids, terpenoids, and tannins among others and identified by characteristic color changes. The test was confirmed the presence of photochemical ingredient as shown in Table 1.

Characterization of synthesized Ag/Fe/ZnO NCs

The synthesized Ag–Fe–ZnO nanocomposite was characterized by its size, shape, surface area, and disparity using sophisticated instruments UV–Visible spectroscopy, FTIR, XRD, DLCS, and SEM.

UV–Visible spectroscopy

UV–visible spectroscopy is an important technique to determine the formation and stability of metal nanoparticle. The optical properties of synthesized Ag/Fe/ZnO NCs were determined by UV–Visible spectroscopy in a range of 200–800 nm to observe their absorption at the specified wavelength. Therefore, when light source applied to the solution, the amount of transmitted in the solution shows the number of electrons excited from doped NCs. The optical properties of Ag/Fe/ZnO was expressed by UV–Vis spectroscopy as shown in the Fig. 1 depicts that broader absorption spectrum over the range peaks were found in the 375–450 nm regions. The characteristic absorbance peak

Table 1 Experimental results of phytochemical screening of leaf extracts

S/N	Phytochemicals	Test	Result
1	Alkaloids	Wagner's test	Positive
2	Flavonoids	Alkaline reagent test	Positive
3	Polyphenol	Ferric chloride test	Positive
4	Tannins	Braymer's test	Positive
5	Terpenoids	Salkowski test	Positive
6	Glycosides	Liebermann's test	Positive
7	Saponins	Foam test	5 cm ~ Positive

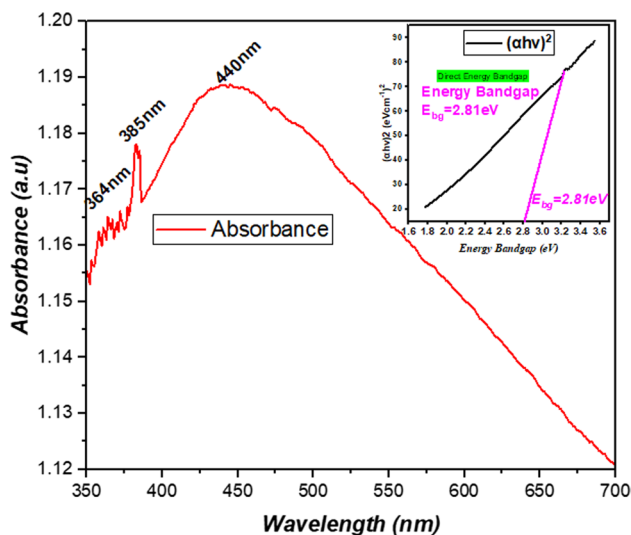


Fig. 1 UV–Visible absorption spectra of Ag/Fe/ZnO NCs

observed at about 328 nm, 385 nm indicated an ultra-small particles size formation, and 440 nm shifted toward longer wavelengths and broadens with increasing nanoparticle size. The bandgap energy of AgNPs, Fe₂O₃NPs, and ZnONPs reported previous was greater than bandgap energy of Ag/Fe/ZnO NCs of current work. These indicated in photocatalytic activity of Ag/Fe/ZnO NCs required minimum amount of energy to excited elector form vacant band to covalent band. The determination of the bandgap energy showed a shift to the visible region in doped samples (2.81 eV). These shows improved efficiency of visible light-harvesting makes Ag/Fe/ZnO NCs suitable candidates for photocatalytic applications. Therefore, the obtained result was confirmed by previous studied (Hoseinpour et al. 2017; Kolya & Kang 2022; Nhi et al. 2022; Rajendran & Sengodan 2017).

Fourier transmissions infrared spectroscopy (FTIR).

The broad/sharp and weak/strong peaks spectra of transmission vs wavenumber on FTIR graph represent the bond of atoms that indicate the functional groups of nanocomposite formation. Figure 2 indicates that the green synthesized Ag/Fe/ZnO NCs peaks were obtained at 425, 564, 699, 878, 1429, and 1632 cm⁻¹ wavenumber. A weak short peak at 425 cm⁻¹ appears indicating the bond of Zn–O formation (Afzal et al. 2022; Bharathi et al. 2019). The medium broad peak at 564 cm⁻¹ indicated the bond of Fe–O formation. At 699 cm⁻¹, assigned alkyl halides compounds indicate the presence (–C–Cl) from the precursor. 878 cm⁻¹ and at 1442 cm⁻¹ indicate –C=C bond. 1631 cm⁻¹ and 1773 cm⁻¹ peak assigned to C=O and C–O stretching indicate the presence of tertiary amides alcohol and phenols that are used for capping organic molecules in nanoparticles, phenols

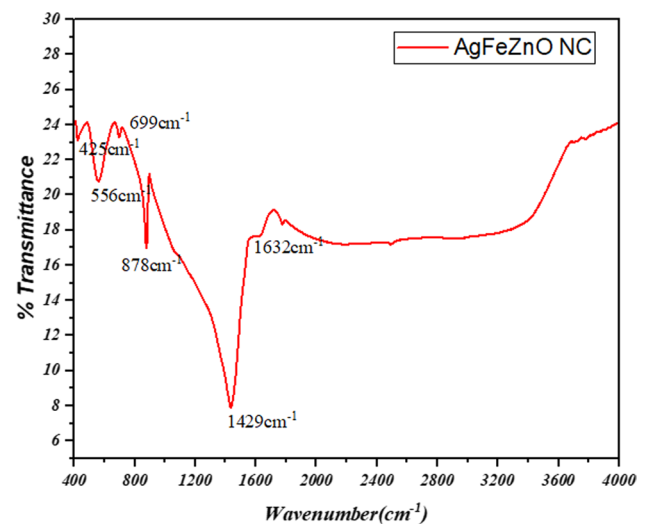


Fig. 2 FTIR spectral analysis of Ag/Fe/ZnO nanocomposite

and amines compounds present in the leaf extract that are responsible for reduction of silver, iron and zinc ion and stability of NCs formed. However, above the 2000 cm⁻¹, there is no peak indicating free from water and other. This result is the same within previous study (Khan et al. 2018; Tolouietabar et al. 2020). The peaks represent stretching and bending of atom that indicated the functional groups of nanocomposite formation.

Dynamic light scattering

The DLS measurement is the most technique used to identify size distribution and disparity of synthesized nanocomposite. The result in Fig. 3 shows the average particle size of distribution 42.276 nm Ag/Fe/ZnO of nanocomposite, which observed from the appearance of one peak with a 100% intensity and 4.265 nm standard deviation. In addition, PDI is 0.183, which shows high stability of NCs. On this graph only one peak and the result indicate monodispersed and homogeneity of Ag/Fe/ZnO of nanocomposite. This result was confirmed with previous study (Ayinde et al. 2020).

X-Ray diffraction spectroscopy (XRD).

The crystalline nature of the green synthesized Ag–Fe–ZnO NCs were characterized by XRD. The patterns of XRD were recorded using a diffract meter by Cu anode material within radiation ($\lambda = 0.154060$ nm) from 10° to 90° angle within tube current was 15 mA and its voltage was 40 kV at 25°C temperature. As it shown in Fig. 4, the patterns for the Ag/Fe/ZnO NCs sample have distinct strong diffraction peaks at 2 θ observed were 28.75°, 32.02°, 34.55°, 38.42°, 40.05°, 44.50°, 45.72°, 56.87°, 64.87°, 75.5° and 77.8° on the plane suggested that the Ag/Fe/ZnO NCs formed was

Fig. 3 DLS result for Ag-Fe/ZnO NCs

	Size (d.nm):	% Intensity:	St Dev (d.nm):
Z-Average (d.nm): 42.27	Peak 1: 43.76	100.0	4.265
Pdl: 0.183	Peak 2: 0.000	0.0	0.000
Intercept: 0.729	Peak 3: 0.000	0.0	0.000

Result quality : Refer to quality report

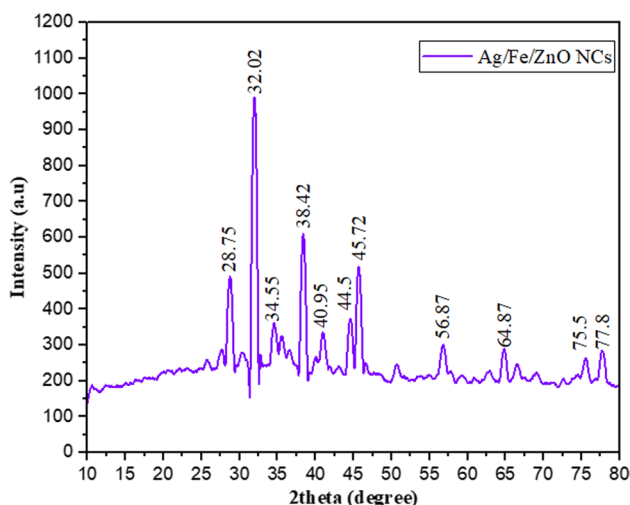
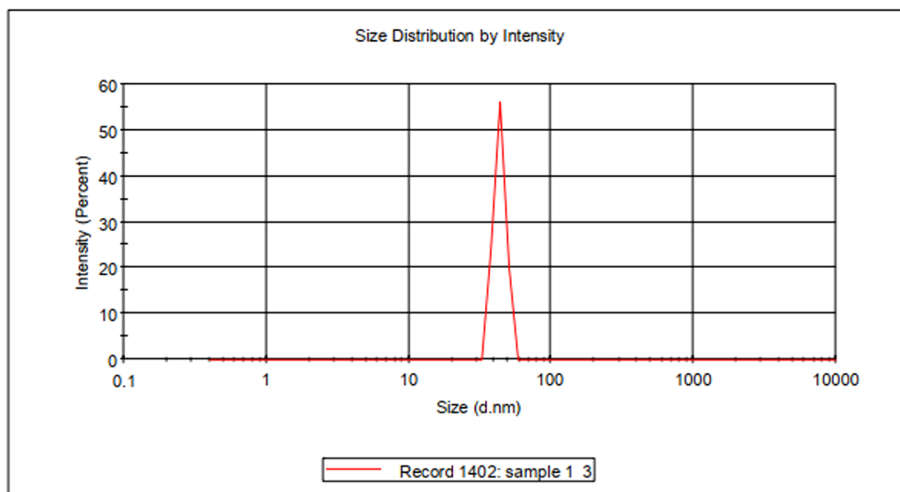


Fig. 4 XRD spectra for Ag/Fe/ZnO NCs

ordered crystalline structure. The average crystallite size of Ag/Fe/ZnO NCs corresponding to the most intense diffraction peak was calculated by the Debye–Scherer formula. The XRD result show the presence and formation of Ag/Fe/ZnO NCs at optimum parameter which have average crystallite size 26.456 nm within cubic crystalline nature that confirm the synthesized nanoparticles were crystalline nature. The obtained result was very close to previously studied (Khorshidi et al. 2016; Kumar & Pandey 2017).

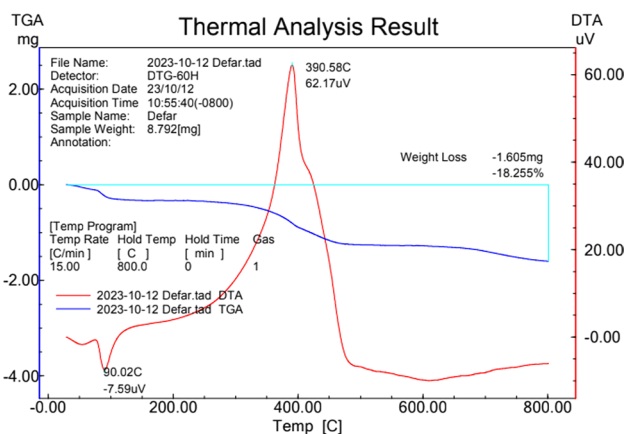


Fig. 5 Thermal gravimetric analysis and differential thermal analysis (TGA and DTA) of Ag/Fe/ZnO NCs

Thermal gravimetric analysis and differential thermal analysis (TGA and DTA)

Figure 5 shows the TGA and DTA results of Ag/Fe/ZnO NCs in the temperature 0–850°C range. The weight loss of Ag/Fe/ZnO NCs was observed from TGA spectrum in 90°C, 380–450, and 750–800°C. This loss is due to evaporation of water molecule and ignition of organic material. However, there is almost no weight loss around 100–380°C and 500–750°C temperature range. DTA spectrum result displays one exothermic peak at 390°C (Khan et al. 2018).

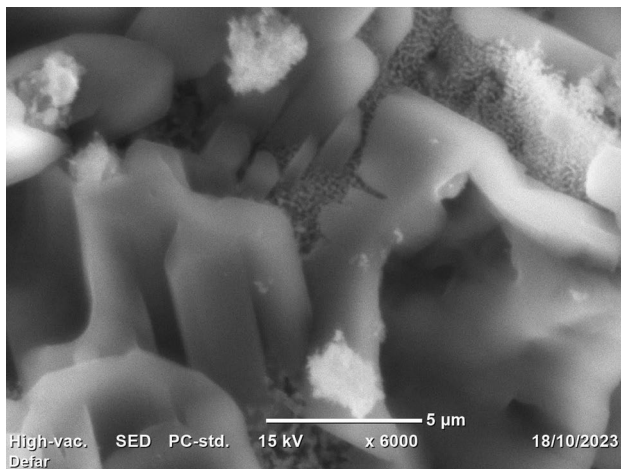


Fig. 6 Photocatalytic degradation of a Amoxicillin using Ag/Fe/ZnONCs

Scanning electron microscope (SEM)

The morphology, particle size and shape of green synthesized Ag/Fe/ZnO NCs were investigated by SEM analysis. As it shown in Fig. 6, the shape of the Ag/Fe/ZnO NCs most likely spherical morphology. However, due to some aggregation of particle the shape is approach to cylindrical morphology. The small size of Ag and Fe-metal coated on the ZnO surface that created Ag–Fe–ZnO NCs rod shape. The result agreed with the size measured by DLS which was 49.19 nm and XRD indicated the average crystal size of 26.456 nm. The SEM image indicate average particle size of Ag/Fe/ZnO NCs is 49.1 nm within 50.1 nm² mean surface area that confirm DLS and XRD data.

BET surface area analysis

The specific surface area of green synthesis of Ag/Fe/ZnO NCs was investigated by Brunauer–Emmett–Teller (BET) analysis. As it shown in Fig. 7, the N₂ adsorption/desorption isotherms plotted for Ag/Fe/ZnO NCs, and the surface area was found to be 8.2 m²/g. This is indicated that relative pressure (P/P₀) from 0.5 to 0.9 increased the surface area of the sample due to the presence of a heterogeneously distributed mesoporous nature of particle. Likewise, a reduction in crystallite size is thought to be the cause of Ag/Fe/ZnO NCs' increased surface area. Therefore, it implies that Ag/Fe/ZnO NCs adsorb pharmaceutical molecules and other contaminants more strongly because of their larger surface area, which increases the percentage of degradation. In addition to this, the average pore diameter and a total pore volume of Ag/Fe/ZnO NCs is found to be 15.224 nm and of 0.0336 cm³/g, respectively. The entire pore volume, average pore diameter, and BET surface area of Ag/Fe/ZnO NCs

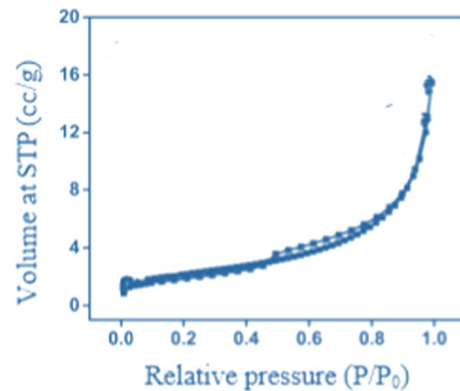


Fig. 7 BET surface area plot from nitrogen adsorption/desorption isotherms for Ag/Fe/ZnO NCs

were seen to have increased, and its mesopore structure was validated by the determined textural parameter values.

Statistical experimental analysis of amoxicillin degradation using synthesized Ag/Fe/ZnO NCs

Table 2 displays the variables that significantly affected the photocatalytic degradation efficiency based on the analysis of variance (ANOVA). This table provided a summary of each model's significant coefficients of response and responses from respondents were highly significant ($p < 0.0001$), and statistical studies show that the design models provide a good fit to the data. The photocatalytic degradation efficiency using green synthesized of Ag/Fe/ZnO NCs of *Embelia schimperia* leaf extract indicated by the Model F value of 1253.35, which suggests the model is important. A, B, C, AC, A², B², C², and D² were discovered to have a substantial impact on the photocatalytic degradation efficiency.

Influence of process parameter on the amoxicillin photocatalytic degradation efficiency

The result of process parameter, Ag/Fe/ZnO NCs dosage, Amoxicillin dosage and time on the amoxicillin Photocatalytic Degradation efficiency was analyzed using central composite design experiment as shown in Table 3. Result depicts that minimum efficiency of 72.18% was obtained at 75 mg of Ag/Fe/ZnO NCs dosage, 40 mg/L of Amoxicillin dosage and 120 min of time. In contrast, the maximum photocatalytic degradation efficiency of 98.5% was obtained at 100 mg of Ag/Fe/ZnO NCs dosage, 30 mg/L of Amoxicillin dosage and 180 min of time. The optimization solutions for maximum yield are shown in Table 3 by using categorical factors.

As can be seen in Fig. 8a–c, the effects Ag/Fe/ZnO NCs dosage, Amoxicillin dosage and time on the amoxicillin photocatalytic degradation efficiency were studied.

Table 2 Analysis of variance for response surface quadratic model of synthesized Ag/Fe/ZnO NCs on amoxicillin photocatalytic degradation efficiency

Source	Sum of square	df	Mean Square	F-value	P-value	
Model	1387.77	9	154.20	1253.35	<0.0001	significant
A–Ag/Fe/ZnO NCs dosage	232.60	1	232.60	1890.65	<0.0001	
B–Amoxicillin dosage	132.91	1	132.91	1080.31	<0.0001	
C–Time	663.96	1	663.96	5396.79	<0.0001	
AB	0.3757	1	0.3757	3.05	0.1111	
AC	46.68	1	46.68	379.39	<0.0001	
BC	0.3512	1	0.3512	2.86	0.1220	
A ²	75.13	1	75.13	610.63	<0.0001	
B ²	52.45	1	52.45	426.32	<0.0001	
C ²	232.96	1	232.96	1893.51	<0.0001	
Residual	1.23	10	0.1230			
Lack of Fit	1.23	5	0.2461			Not significant
Pure Error	0.0000	5	0.0000			
Cor Total	1389.01	19				

Table 3 Experimental results of photocatalytic degradation efficiency

Run	Ag/Fe/ZnO NCs dosage, mg	Amoxicillin dosage, mg/L	Time, min	Photocatalytic Degradation efficiency, %
1	100	30	180	98.5
2	75	40	120	95
3	50	50	180	89
4	50	40	120	81.688
5	50	50	60	70
6	100	40	120	95.82
7	75	40	120	95
8	100	50	180	92.1354
9	50	30	60	76.3359
10	75	40	120	95
11	50	30	180	95
12	100	30	60	90
13	75	50	120	85
14	75	40	120	95
15	100	50	60	82.295
16	75	40	120	95
17	75	40	180	95.5
18	75	40	120	94.6318
19	75	40	120	95
20	75	40	120	72.18

According to the curve in Fig. 8a, the photocatalytic degradation efficiency increased noticeably from 72.5 to 98.5% as the Ag/Fe/ZnO NCs dosage from 50 to 100 mg. Above 75 mg, there has been a modest increase in degradation efficiency, showing that using high Ag/Fe/ZnO NCs dosage has little impact. The effective Ag/Fe/ZnO NCs dosage is 75 mg with a slight rise in degradation efficiency, according to the experimental results of the photocatalytic

amoxicillin degradation as a function of Ag/Fe/ZnO NCs dosage analysis. Figure 8b illustrates the effect of Amoxicillin dosage on the photocatalytic amoxicillin degradation in addition to the effect of Ag/Fe/ZnO NCs dosage, showing that the maximum efficiency was achieved at 30 mg/L of amoxicillin concentration, which was 98.5%, and that it significantly decreased to 89% as the concentration of Amoxicillin dosage was increased to 50 mg/L. This was due to photocatalyst’s reduced active sites for the oxidation of the amoxicillin molecule. Higher starting concentrations of amoxicillin resulted in more reactants and reaction intermediates being absorbed at the photocatalyst level, which meant that there was not enough hydroxyl radical available to decompose amoxicillin at higher concentrations (Bayisa et al. 2023; Kumar & Pandey 2017). When its concentrations increased, its rate of decomposition was decreased.

Thus, it is evident to say that variations in the concentration of Amoxicillin beyond 50 mg/L instigated changes in the photocatalytic degradation efficiency of amoxicillin to vary, showing that using the concentration of amoxicillin has significant effect on the degradation effect. Additionally, the effect’s reaction time was studied since the photocatalytic efficiency varies with their values. Figure 8c revealed that the Amoxicillin degradation increased (about 72.5 to 98.5%) with increasing radiation time (60, 120, and 180 min). Nonetheless, the reaction’s initial 60 min saw the maximum degrading efficiency, after which its upward trend constant. This may be explained by the quick breakdown of Amoxicillin contamination in the 60 min prior to the reactivity of free radicals produced by the applied electron excitation. Herein, *Embelia schimperia* leaf extract was subjected to acidic and slightly basic conditions in order to analyze the development of Ag/Fe/ZnO nanocomposites. This might be explained by the fact that some *Embelia schimperia* leaf

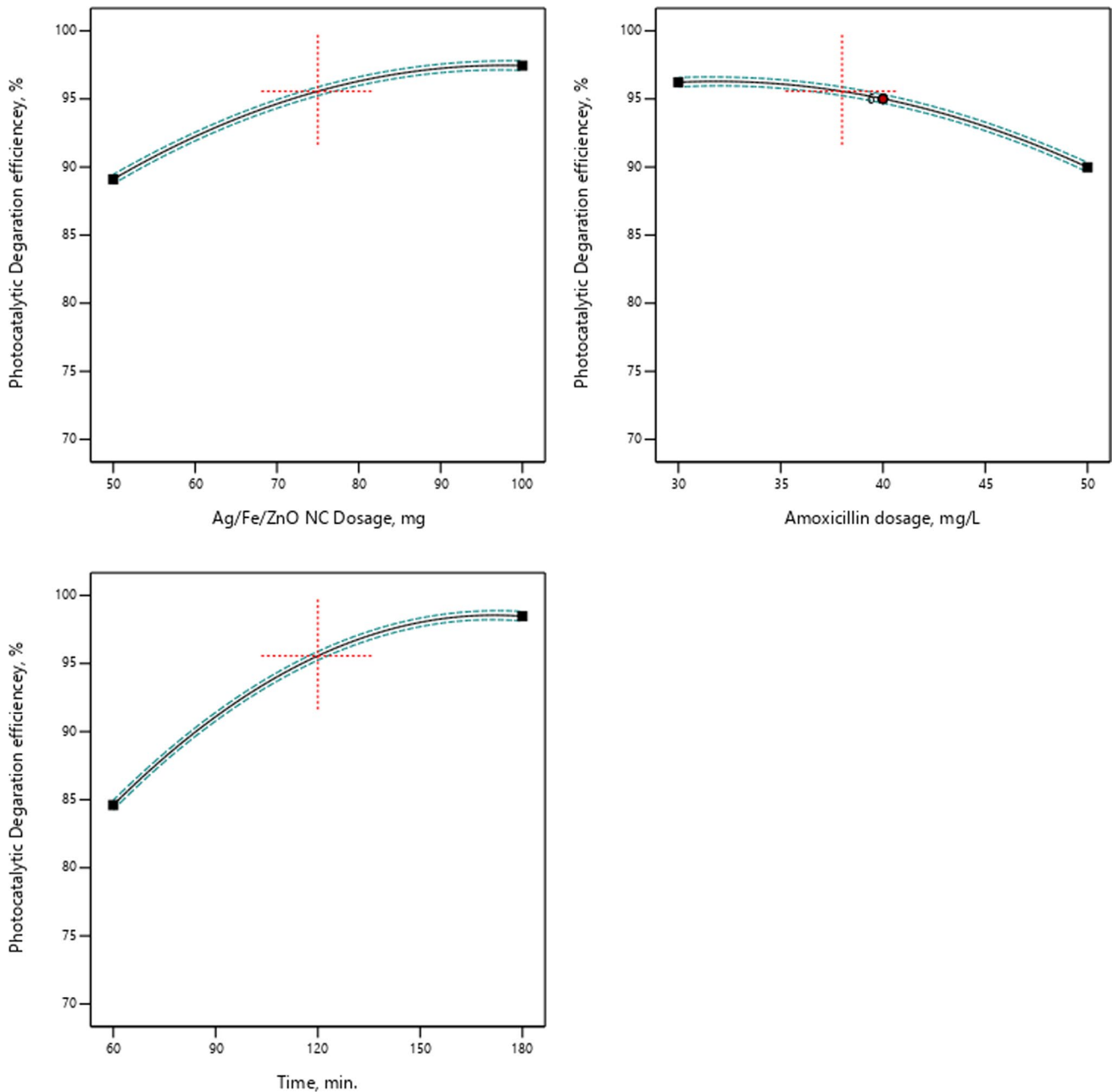


Fig. 8 Effects of **a** Ag/Fe/ZnO NCs dosage, **b** Amoxicillin dosage and **c** radiation time on the amoxicillin photocatalytic degradation efficiency

extract phytocompounds release OH ions when they are oxidized in the presence of metal precursor ions (Bayisa & Bultum 2022).

Amoxicillin photocatalytic degradation

The photocatalytic degradation of Amoxicillin took place for 150 min applying 15 LED light source to active catalytic surface by formation electron and hole. As shown in Fig. 9, the initial concentration of Amoxicillin is relatively high (0.79) at 0 min, and there was some degradation in the dark

case for 30 min. However, after 30 min of 15 W LED light used, the concentration/absorbance of Amoxicillin reduced and then gradually decreased, and as time moved to the final 150 min, the absorbance and concentration decreased. This drop in concentration/absorbance is due to the catalytic surface receiving light/photon energy from a 15 W LED source, where electrons escape from the valance band to the covalent band as negative charge and holes as positive charge, which is responsible for the degradation of the Amoxicillin. When the interaction period is departed, the electron and holes regenerate. When contact time increased, the reformation of

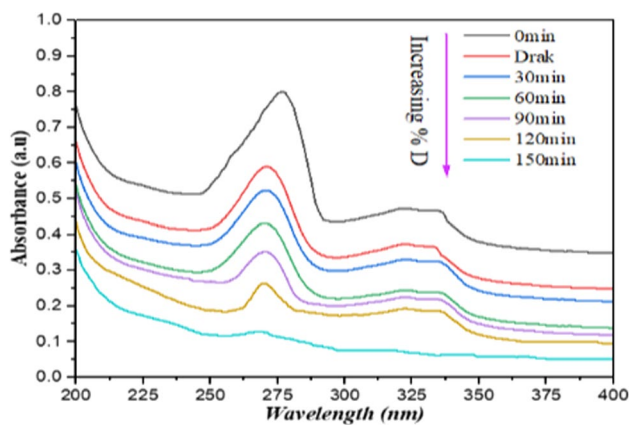


Fig. 9 UV–visible data for removal of Ciprofloxacin using Ag/Fe/ZnO NCs

electron and hole regenerates. As the result, the Amoxicillin degraded to non-toxic carbon dioxide and water molecule. Therefore, the efficiency of Ag/Fe/ZnO NCs calculated is 98.5% for degradation of Amoxicillin drugs.

Conclusion

In this study, green Ag/Fe/ZnO NCs from *Embelia schimperia* leaf extract were successfully produced for *Photocatalytic Degradation of amoxicillin* using a straightforward co-precipitation technique. The synthesized Ag/Fe/ZnO photocatalyst was characterized and validated by FTIR, XRD, UV–vis, DLS, TGA, SEM and DTA analysis. Using a response surface methodology of central composite design, the impact of green synthesized Ag/Fe/ZnO NCs dosage, Amoxicillin dosage and radiation time on the photocatalytic degradation of Amoxicillin was examined. Thus, the natural *Embelia schimperia* leaf extract played a significant role in the increasing of photocatalytic properties at the Ag–Fe–ZnO nanocomposite, which leads to photocatalyst's reduced active sites for the oxidation of the amoxicillin molecule. Approximately 98.5% of Amoxicillin has been eliminated after 180 min in the presence of Ag–Fe–ZnO under visible light.

Acknowledgements We would like to acknowledge the FTIR, XRD analysis and UV–vis spectrum platform at the Faculty of Material Science and Engineering, and the school of Chemical Engineering Laboratory staff members at Jimma Institute of Technology for their knowledge-sharing and technical support. This work was financially supported by the Jimma Institute of Technology Center of Excellence-CRGE RESOURCE CART (Climate Resilient Green Economy Resource Centre for Advanced Research and Training-Linking Energy with Water and Agriculture).

Author contributions All authors contributed to the conceptualization of the research and writing the manuscript. All authors read and

approved the final manuscript. DGG involved in writing—original draft preparation and data creation. YMB involved in conceptualization, methodology, and investigation. EBJ, TTT, and TAB involved in writing—review and editing, investigation, analysis, supervision, and visualization.

Funding The author(s) received no specific funding for this work.

Declarations

Conflict of interest The authors declare that they have no competing interests.

Ethical approval The authors have complied with all ethical standards while writing the article and conducting the research.

Open Access This article is licensed under a Creative Commons Attribution-NonCommercial-NoDerivatives 4.0 International License, which permits any non-commercial use, sharing, distribution and reproduction in any medium or format, as long as you give appropriate credit to the original author(s) and the source, provide a link to the Creative Commons licence, and indicate if you modified the licensed material. You do not have permission under this licence to share adapted material derived from this article or parts of it. The images or other third party material in this article are included in the article's Creative Commons licence, unless indicated otherwise in a credit line to the material. If material is not included in the article's Creative Commons licence and your intended use is not permitted by statutory regulation or exceeds the permitted use, you will need to obtain permission directly from the copyright holder. To view a copy of this licence, visit <http://creativecommons.org/licenses/by-nc-nd/4.0/>.

References

- Afolalu SA, Ikumapayi OM, Ogedengbe TS, Kazeem RA, Ogundipe AT (2022) Waste pollution, wastewater and effluent treatment methods—An overview. *Mater Today: Proc* 62:3282–3288
- Afzal G, Jamal A, Kiran S, Mustafa G, Ahmad F, Saeed S, Ahmad H, Dawood S (2022) *Aerva javanica* mediated synthesis, characterization and antimicrobial evaluation of zinc oxide nanoparticles. *Japs: J Animal Plant Sci* 32(2):5
- Alwhibi MS, Soliman DA, Awad MA, Alangery AB, Al Dehaish H, Alwasel YA (2021) Green synthesis of silver nanoparticles: characterization and its potential biomedical applications. *Gr Process Synth* 10(1):412–420
- Aththanayaka S, Thiripuranathar G, Ekanayake S (2022) Emerging advances in biomimetic synthesis of nanocomposites and potential applications. *Mater Today Sustain* 20:100206
- Ayinde W, Gitari W, Munkombwe M, Samie A, Smith JA (2020) Green synthesis of AgMgOnHaP nanoparticles supported on chitosan matrix: defluoridation and antibacterial effects in groundwater. *J Environ Chem Eng* 8(5):104026
- Bayisa YM, Bullo TA (2021) Optimization and characterization of oil extracted from croton macrostachyus seed for antimicrobial activity using experimental analysis of variance. *Heliyon*. <https://doi.org/10.1016/j.heliyon.2021.e08095>
- Bayisa YM, Bullo TA, Akuma DA (2021) Chromium removal from tannery effluents by adsorption process via activated carbon chat stems (*Catha edulis*) using response surface methodology. *BMC Res Notes* 14:1–6
- Bayisa YM, Bullo TA, Hundie KB, Akuma DA, Gizachew DG, Bultum MS (2023) Ecofriendly green synthesis and characterization of silver zinc oxide nanocomposite using the aqueous leaf extract

- of rumex crispus: evaluation of its antimicrobial and antioxidant activity. *Heliyon* 9(5):6
- Bayisa YM, Bultum MS (2022) Extraction of oil from maesa lanceolata seeds and evaluation of its antimicrobial activities. *S Afr J Chem Eng* 40(1):126–133
- Bayisa YM, Teso WA (2021) Solid sulfonated silica acid catalyst for epoxidation of podocarpus falcatus seed oil. *Biomass Convers Biorefinery* 3:1–10
- Bharathi D, Ranjithkumar R, Chandarshekar B, Bhuvaneshwari V (2019) Preparation of chitosan coated zinc oxide nanocomposite for enhanced antibacterial and photocatalytic activity: as a bionanocomposite. *Int J Biol Macromol* 129:989–996
- Biswal SK, Panigrahi GK, Sahoo SK (2020) Green synthesis of Fe₂O₃-Ag nanocomposite using Psidium guajava leaf extract: an eco-friendly and recyclable adsorbent for remediation of Cr (VI) from aqueous media. *Biophys Chem* 263:106392
- Bozorg-Haddad O, Delpasand M, Loáiciga HA (2021) Water quality, hygiene, and health. In: Bozorg-Haddad O (ed) *Economical, political, and social issues in water resources*. Elsevier, UK, pp 217–257
- Bullo TA, Bayisa YM (2022) Optimizing the removal efficiency of chromium from tanning plant effluent by adsorption method with activated carbon chat stems (*catha edulis*) using response surface methodology. *Water Conser Manag (WCM)* 6(1):15–21
- Costa F, Lago A, Rocha V, Barros O, Costa Vipotnik Silva Tavares LZBT (2019) A review on biological processes for pharmaceuticals wastes abatement—a growing threat to modern society. *Environ Sci Technol* 53(13):7185–7202
- Hoseinpour V, Soury M, Ghaemi N, Shakeri A (2017) Optimization of green synthesis of ZnO nanoparticles by *Dittrichia graveolens* (L.) aqueous extract. *Health Biotechnol Biopharm* 1(2):39–49
- Immanuel S, Aparna T, Sivasubramanian R (2019) Graphene–metal oxide nanocomposite modified electrochemical sensors. In: Alagarsamy Pandikumar, Perumal Rameshkumar (eds) *Graphene-based electrochemical sensors for biomolecules*. Elsevier, UK, pp 113–138
- Ishak NM, Kamarudin S, Timmiati S (2019) Green synthesis of metal and metal oxide nanoparticles via plant extracts: an overview. *Mater Res Express* 6(11):112004
- Jeevanandam J, Kiew SF, Boakye-Ansah S, Lau SY, Barhoum A, Danquah MK, Rodrigues J (2022) Green approaches for the synthesis of metal and metal oxide nanoparticles using microbial and plant extracts. *Nanoscale* 14(7):2534–2571
- Khan M, Tareq F, Hossen M, Roki M (2018) Green synthesis and characterization of silver nanoparticles using *Coriandrum sativum* leaf extract. *J Eng Sci Technol* 13(1):158–166
- Khan NA, Ahmed S, Farooqi IH, Ali I, Vambol V, Changani F, Yousefi M, Vambol S, Khan SU, Khan AH (2020) Occurrence, sources and conventional treatment techniques for various antibiotics present in hospital wastewaters: a critical review. *TrAC, Trends Anal Chem* 129:115921
- Kharissova OV, Kharisov BI, Oliva González CM, Méndez YP, López I (2019) Greener synthesis of chemical compounds and materials. *Royal Soc Open Sci* 6(11):191378
- Khorshidi N, Khorrami S, Olya M, Mottiee F (2016) Photodegradation of basic dyes using nanocomposite (silver zinc oxide-copper oxide) and kinetic studies. *Orient J Chem* 32(2):1205–1214
- Kolya H, Kang C-W (2022) Biogenic synthesis of silver-iron oxide nanoparticles using kulekhara leaves extract for removing crystal violet and malachite green dyes from water. *Sustainability* 14(23):15800
- Kumar A, Pandey G (2017) A review on the factors affecting the photocatalytic degradation of hazardous materials. *Mater Sci Eng Int J* 1(3):1–10
- Mekonnen Y (2021) Epoxidation of podocarpus falcatus oil by sulphuric acid catalyst: process optimization and physico-chemical characterization. *Am J Chem Eng* 9(4):84–90
- Nhi TTY, Thien DT, Cong TD, Tung NT, Thuy LT, Nu TT, Dat ND, Hileuskaya K, Kalatskaja J (2022) Green synthesis of pectin-silver nanocomposite: parameter optimization and physico-chemical characterization. *Vietnam J Chem* 60:66–71
- Pandit AB, Kumar JK (2019) Drinking water treatment for developing countries: physical, chemical and biological pollutants. *Royal Soc Chem*
- Rajendran SP, Sengodan K (2017) Synthesis and characterization of zinc oxide and iron oxide nanoparticles using *Sesbania grandiflora* leaf extract as reducing agent. *J Nanosc* 2017:1
- Salem SS, Fouda A (2021) Green synthesis of metallic nanoparticles and their prospective biotechnological applications: an overview. *Biol Trace Elem Res* 199:344–370
- Samal K, Mahapatra S, Ali MH (2022) Pharmaceutical wastewater as Emerging Contaminants (EC): treatment technologies, impact on environment and human health. *Energy Nexus* 6:100076
- Sharma, M., Kalita, P., Senapati, K. K., & Garg, A. (2018). Study on magnetic materials for removal of water pollutants. *Emerging pollutants-some strategies for the quality preservation of our environment*, 61–78.
- Siddiqui Shah DUR-RE-SHAHWARALIMMUZAMMILFATIMA MNMSYAN (2021) The phytochemical analysis of some medicinal plants. *Liaquat Med Res J* 3(1):1
- Singh J, Dutta T, Kim K-H, Rawat M, Samddar P, Kumar P (2018) ‘Green’ synthesis of metals and their oxide nanoparticles: applications for environmental remediation. *J Nanobiotechnol* 16(1):1–24
- Tolouietabar H, Hatamnia AA, Sahraei R, Soheyli E (2020) Biologically green synthesis of high-quality silver nanoparticles using *Scrophularia striata* Boiss plant extract and verifying their antibacterial activities. *J Nanostructures* 10(1):44–51
- Yadav R, Agarwala M (2011) Phytochemical analysis of some medicinal plants. *J Phytol* 3(12):10–14

Publisher's Note Springer Nature remains neutral with regard to jurisdictional claims in published maps and institutional affiliations.